Heliyon 10 (2024) e33133

Contents lists available at ScienceDirect

Heliyon

journal homepage: www.cell.com/heliyon

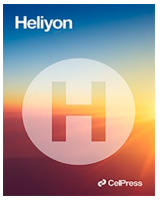

Research article

Evaluating the effect of tissue stimulation at different frequencies on breast lesion classification based on nonlinear features using a novel radio frequency time series approach

Elaheh Norouzi Ghehi [a], Ali Fallah [a,*], Saeid Rashidi [b], Maryam Mehdizadeh Dastjerdi [a]

[a] Faculty of Biomedical Engineering, Amirkabir University of Technology, Tehran, Iran
[b] Faculty of Medical Sciences and Technologies, Science and Research Branch, Islamic Azad University, Tehran, Iran

ARTICLE INFO

Keywords:
Breast lesion classification
Dynamic tissue stimulation
Nonlinear features
PVA phantoms
RFTSDP method
Ultrasound radio frequency time series

ABSTRACT

Objective: Radio Frequency Time Series (RF TS) is a cutting-edge ultrasound approach in tissue typing. The RF TS does not provide dynamic insights into the propagation medium; when the tissue and probe are fixed. We previously proposed the innovative RFTSDP method in which the RF data are recorded while stimulating the tissue. Applying stimulation can unveil the mechanical characteristics of the tissue in RF echo.

Materials and methods: In this study, an apparatus was developed to induce vibrations at different frequencies to the medium. Data were collected from four PVA phantoms simulating the nonlinear behaviors of healthy, fibroadenoma, cyst, and cancerous breast tissues. Raw focused, raw, and beamformed ultrafast data were collected under conditions of no stimulation, constant force, and various vibrational stimulations using the Supersonic Imagine Aixplorer clinical/research ultrasound imaging system. Time domain (TD), spectral, and nonlinear features were extracted from each RF TS. Support Vector Machine (SVM), Random Forest, and Decision Tree algorithms were employed for classification.

Results: The optimal outcome was achieved using the SVM classifier considering 19 features extracted from beamformed ultrafast data recorded while applying vibration at the frequency of 65 Hz. The classification accuracy, specificity, and precision were 98.44 ± 0.20 %, 99.49± 0.01 %, and 98.53± 0.04 %, respectively. Applying RFTSDP, a notable 24.45 % improvement in accuracy was observed compared to the case of fixed probe assessing the recorded raw focused data.

Conclusions: External vibration at an appropriate frequency, as applied in RFTSDP, incorporates beneficial information about the medium and its dynamic characteristics into the RF TS, which can improve tissue characterization.

1. Introduction

Breast cancer is a prevalent global diagnosis, underscoring the importance of early detection for expediting healing [1]. Ultrasound (US) has emerged as a widely used medical imaging modality, surpassing MRI and X-ray in safety and portability [2]. However,

* Corresponding author.
E-mail addresses: norouzi1495@aut.ac.ir (E. Norouzi Ghehi), afallah@aut.ac.ir (A. Fallah), rashidi.saeid@srbiau.ac.ir (S. Rashidi), mmehdizadehd@aut.ac.ir (M. Mehdizadeh Dastjerdi).

https://doi.org/10.1016/j.heliyon.2024.e33133
Received 10 January 2024; Received in revised form 13 June 2024; Accepted 14 June 2024
Available online 20 June 2024

challenges in US-based diagnosis include low contrast in high speckle brightness mode images and operator variability [3]. Despite the efficacy of conventional imaging, diagnosing benign or malignant breast lesions often requires invasive tissue biopsies, prompting a need for a non-invasive, low-cost, portable, and accurate method [4].

The correlation between tissue mechanical property changes and diseases has led to the development of elastography methods, focusing on tissue elasticity [5,6]. Recent studies exploring nonlinear models to mimic tissue behavior acknowledge limitations, including a lack of very high accuracy, relative elastic coefficients (especially for breast tissues), and high calibration costs [7]. Addressing these challenges is vital for advancing the accuracy and accessibility of breast tissue characterization methods.

An US-based method was proposed by Moradi et al., in 2006 to capture a sequence of RF frames from a stationary tissue location, creating RF TS. This approach relies on continuous interactions between the tissue and US waves, where the reconstructed TS of echoes carries valuable information about the tissue [8]. The versatility of RF signals extends to various goals, including tissue elasticity imaging, blood flow imaging [9], radiation force impulse imaging [10], non-invasive temperature estimation, and tissue characterization [11]. Importantly, the use of RF TS eliminates the need for modeling tissue or calculating model parameters [12,13].

Moradi et al. conducted an extensive investigation of RF TS on phantom, animal, ex-vivo, and in-vivo prostate tissues, demonstrating its efficacy in animal tissue typing and prostate tissue classification [2,8,14–19]. Notably, the authors highlighted that their most successful outcomes were achieved by employing six spectral features and incorporating the fractal dimension, using SVM classifiers [5,13–20]. A related study by Aboofazeli et al. explored discrete wavelet transform for RF TS analysis but found no significant improvement compared to the spectral and fractal properties [12]. The impact of US imaging parameters, including transmission power and frame rate, on tissue classification was studied [14]. Imani et al. investigated the influence of region of interest (ROI) size and RF TS length, revealing that optimal classification results were associated with larger ROI sizes and longer RF TS lengths [17].

Researchers focused on breast tissue classification using RF TS, employing SVM and Random Forest algorithms to categorize breast tissues into cancerous and normal classes [2]. Recent studies have advanced toward combining elasticity with other US-based methods. Brock et al. introduced a multiparametric approach, combining contrast-enhanced US with real-time elastography, demonstrating a significant reduction in false-positive rates compared to elastography alone [21].

In our previous studies, we introduced a novel method called RF Time Series Dynamic Processing (RFTSDP), which combines elastography principles with RF TS to improve tissue characterization [22,23]. RFTSDP involves capturing information from the signal during tissue excitation, showcasing the potential for enhanced feature extraction. Importantly, this method does not necessitate sophisticated equipment or complex calculations, suggesting its potential as a simple, non-invasive, low-cost, and online method for distinguishing tissue types.

Using agar-gelatin-based phantoms to simulate normal and cancerous breast tissue, our analysis of three recorded data types revealed that employing RFTSDP with vibrational stimulation improved classification performance [22]. The study also investigated the impact of recording parameters, such as depth and probe central frequency, on classification outcomes [23]. Optimal classification accuracy was achieved through vibrational stimulation and 6.4 MHz probe central frequency in beamformed ultrafast data. These findings underscore the potential of innovative approaches in advancing the accuracy and practicality of tissue classification methods.

The potential of RF TS in tissue typing and information extraction has been recognized in various applications, such as determining liver tissue fibrosis and its stage [24], early prediction of breast tumor response to chemotherapy [25], distinguishing high-intensity focused ultrasound (HIFU)-induced thermal lesions from normal tissue [26,27], and thermometry in low-intensity focused ultrasound (LIFU) [28]. Several studies in this field utilized different methods to extract features from RF signals or US images, along with machine learning for breast cancer determination [29,30]. In 2022, a similar method to our proposed approach was applied to classify breast tissue lesions as malignant or benign, representing a novel direction in elasticity imaging for tissue classification [31].

Various methods have been employed to extract features from RF signals or US images, alongside different machine learning techniques for breast cancer determination. Deep learning methods, such as convolutional neural networks (CNNs), have been applied to automatically extract features and develop breast lesion classification and segmentation models [37]. Nakagami parametric images were utilized for the non-invasive classification of breast lesions [38]. The analysis involved exploring different window sizes and features, highlighting the potential of Nakagami images for accurate characterization of breast tissue.

A multi-task network has demonstrated superior performance compared to traditional approaches using B-mode images, indicating the potential of RF data for improved breast mass analysis [35]. In another study [33], a deep learning model achieved superior performance compared to a Nakagami parameter-based classifier, showcasing the feasibility of using RF data for accurate breast mass classification. Additionally, a deep learning framework (SCD-Net) was proposed for automatic calcification detection based on RF signals [34].

Study [32] introduced a multi-class classification strategy that incorporates background tissue as an additional class, resulting in improved invasive ductal carcinoma (IDC) detection. Further studies [36–39] introduced W-Net, UNet, and CNN models, demonstrating the diagnostic capability of RF data for breast tumor detection. In Ref. [40], a three-step image processing scheme was introduced to enhance the generalization of a deep learning model (VGG19) for breast cancer classification. The study showed improved performance on multiple datasets, emphasizing the importance of preprocessing in deep learning models for clinical applications [32–40].

Given the intricate nature of breast tissue compared to prostate tissue, comprehensive tissue typing necessitates a method capable of capturing a richer set of information, particularly pertaining to mechanical properties. Thus, RFTSDP emerges as a promising approach for characterizing breast tissue. To overcome the limitations of applying this method to in-vivo human tissues, the research utilized phantoms mimicking normal and mammary lesions. Previous studies employed agar-gelatin phantoms [22,23], known for their linear mechanical behavior [41,42]. However, to assess RFTSDP's efficacy in reconstructing nonlinear parameters of soft tissues,

phantoms with hyper-elastic behavior were deemed necessary.

The choice of materials for phantoms depends on factors such as the frequency range of the US equipment, practical handling considerations, and the specific part of the human body being simulated. In terms of acoustical properties, polyvinyl alcohol (PVA) stands out as fitting best within breast tissue, especially up to 10 MHz [43]. PVA gels were introduced as photoacoustic phantoms by Kharine et al. [44] and are widely used for photoacoustic imaging and optical elastography. PVA is frequently utilized to create breast phantoms that mimic the nonlinear stress-strain behavior of the tissue [45].

Devi et al. fabricated PVA gel phantoms to closely match the mechanical, optical, and acoustic properties of human breast tissue [46]. This was achieved by adjusting the number of freeze-thaw cycles (FTC) and the degree of hydrolysis of PVA. The resulting acoustic properties, including sound speed, acoustic attenuation coefficient, and density, closely approximated average values reported in the literature for normal breast tissue [46,47]. Therefore, in the present investigation, PVA phantoms were chosen as the optimal simulator for breast tissue and lesions.

Different PVA concentrations and cellulose scatterers were characterized acoustically and thermally by Braunstein et al. (2022). Their findings suggested that PVA cellulose composite hydrogels could effectively mimic acoustic, cavitation, and thermal properties of soft tissues in several US applications [48]. For this purpose, our study utilized cellulose as the scatterer in the phantoms. To implement the proposed idea in RFTSDP, in addition to an external vibrator, we utilized the same US recording equipment that allows for the investigation of raw RF echo and has ultrafast mode which could swiftly track the backscatter movements. In our previous studies, it was found that applying vibration provides more information in RF TS and leads to higher accuracy in tissue classification [22,23]. Therefore, the research on the RFTSDP method continued. The main contributions of the present study are summarized as follows.

- Using various stimulations and vibrations with different frequencies necessitated the design and implementation of a simple vibrator vibrating at desired frequencies.
- Fabricating PVA phantoms to appropriately simulate breast tissue's optical, acoustic, and mechanical properties.
- Distinguishing non-cancerous lesions in addition to healthy and cancerous ones.
- Recording ultrafast data from breast tissues to form RF TS for tissue characterization.
- Extracting nonlinear features from RF TS, such as TD and spectral features, as a result of constructing phantoms with hyper-elastic behavior.
- Applying SVM with five different kernels, Random Forest, and three decision trees as classifiers.

The subsequent sections of this paper are structured as follows: Section 2 addresses the fabrication of phantoms, and vibrator, and data recording conditions. Feature extraction and classification methodologies are outlined in Section 3. Section 4 reported the performance evaluation of the proposed technique, with the discussion of findings detailed in Section 5. Finally, conclusions are presented in Section 6.

2. Materials

The assessment of RFTSDP involves obtaining RF TS from diverse tissues while subjecting the tissues to stimulation. To replicate various breast tissue types—normal, cystic, fibroadenoma, and cancerous—PVA phantoms were employed. Data collection occurred in three modes: raw focused, raw ultrafast, and beamformed ultrafast. Multiple stimulation methods, such as simple mode, static, and vibration at different frequencies, were applied. Relevant features were extracted from chosen ROIs, and classification utilized SVMs with five distinct kernels, a Random Forest, and three decision trees. This section details the processes involved in phantom creation, stimulation application, and vibrator manufacturing.

2.1. Phantoms

PVA powder from Sigma-Aldrich (Catalog No. 36 314-6) served as the base material for constructing the phantoms. The formulation for PVA-based phantoms replicating both normal and cancerous breast tissues has been documented in various studies, with minor variations in the number of FTCs or the proportion of PVA [46,47,49]. In this investigation, we adopted the parameters commonly cited in the literature for fabricating normal and cancerous breast phantoms [50]. Our study involved a comparative analysis of the reported elastic coefficients of cyst and fibroadenoma lesions alongside PVA phantoms with varying FTCs and PVA proportions [44–46,50,51]. Detailed information regarding the numbers of FTCs and material percentages is provided in Table 1.

Table 1
Numbers of FTCs and percentages of materials in four phantoms of normal, fibroadenoma, cyst, and cancerous breast tissues [44–46,50,51].

Mimicking Tissue	Elastic Module (kPa)	PVA (%)	Deionized Water (%)	Cellulose (%)	Biocide (%)	FTC
Normal Tissue	3.25 ± 0.91	5	91.98	3	0.02	2
Fibroadenoma	6.41 ± 2.86	5	91.98	3	0.02	4
Cyst	17.11 ± 7.35	10	86.98	3	0.02	2
Cancer (IDC)[a]	19.99 ± 4.20	10	86.98	3	0.02	5

[a] Infiltrating Ductal Carcinoma.

To make each phantom, based on the percentage mentioned in Table 1, PVA was slowly added to the water in the beaker placed on a hot plate. Care was taken to limit the temperature to no more than 90 °C during this process to prevent PVA burning and the formation of undesirable bubbles in the gel, which could compromise the mechanical properties of the phantom [42]. The relative percentages of cellulose (Sigma Aldrich Corp) were added to the mixture as acoustic scatterers [51]. To keep the phantom at room temperature 0.02 % biocide was added to the solution.

The mixture was then cast in a Perspex mold with dimensions of $5 \times 10 \times 15$ cm^3 for each phantom. The supersonic shear wave elastography imaging capability of the Aixplorer Us system was used to verify the desired elastic coefficients of the phantoms at the end of FTCs. Subsequently, the RF data were recorded under various stimulations.

2.2. Vibrator

In previous studies, a shaver with a constant vibration frequency was used for stimulation, impacting the displacement of phantom scatterers, alterations in RF backscattering patterns, and improving classification results [22,23]. In this research, a customized vibrator was designed with variable frequencies (35–65 Hz), aiming to encompass the dynamic response of the breast tissue. The vibrator implementation involved utilizing a DC motor with a two mm crank. A rod, positioned around the shaft, supports a plate that facilitates the transmission of vibration to the tissue's surface. An Arduino board was employed to generate PWM commands according to the desired speed. The vibrator was secured in a wooden holder for stability, as illustrated in Fig. 1 The RF data were recorded using the vibrator to induce vibrations at several desired frequencies.

2.3. Data sets

RF data were recorded using a Supersonic Imaging Aixplorer clinical/research US System equipped with a SuperLinear™ SL18-5 linear probe. To enhance the influence of dynamic tissue properties on RF echo signals, various stimulation methods were applied, including simple (fixed probe with no force), static (constant force during recording), and vibrational mode. Data collection involved recording in raw and beamformed ultrafast mode, as well as raw in focused mode. The choice of ultrafast mode, with its higher imaging speed and better ability to track movement, was made to capture dynamic tissue responses during vibration.

For static stimulation, a holder with adjustable height was utilized to maintain constant pressure perpendicular to the tissue by the probe. In vibrational stimulation, a vibrator placed two cm from the US probe on the phantom's surface was employed, varying frequencies at 35, 45, 55, and 65 Hz. Recording parameters, including the probe's center frequency (6.4 MHz), image depth (4 cm), and focus at 2 cm depth, were determined based on previous studies [22,23]. The frame rate is set to 100 in focused mode and 5000 in ultrafast mode, time series length is 256 and 50 respectively.

RF data obtained from the Supersonic Imaging device were stored in a specialized format. A MATLAB-based [52] graphical user interface (GUI), named RF Data Parser (Fig. 2), was developed to convert the data into a *mat.* file format and visualize the final B-mode image.

This tool also facilitates the application of various filters to both RF data and B-mode images. The subsequent section details the processes of selecting ROIs, forming TSs, and extracting relevant features. Six distinct stimulation types were conducted, with data recorded in three modes for each type (raw focused, raw, and beamformed ultrafast). Utilizing the RF Data Parser, all 18 datasets were saved as *mat.* files, preparing them for the TS creation.

3. Methods

Previous sections have explained datasets and preprocessing. Section 3 will delve into the discussion of feature selection, feature extraction, and classification. Fig. 3 presents a block diagram representing the proposed method.

Fig. 1. Complete system implemented for vibrating the constructed phantoms.

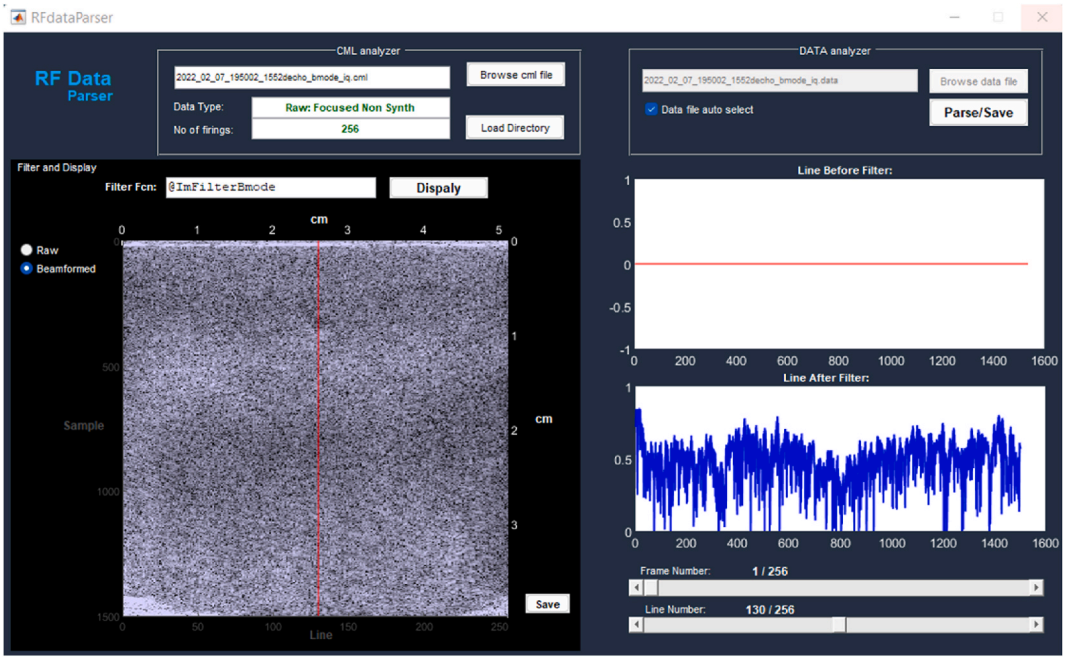

Fig. 2. RF Data Parser, developed GUI to convert our recording data into a *mat*. file format.

3.1. Feature extraction

The data recording process involved selecting two distinct areas on each phantom's surface. Within these regions, eight ROIs were identified at specified depths for each frame. Subsequently, features were extracted from the RF TS within each ROI, with dimensions of 1 mm × 3.5 mm. This resulted in a total of 16 ROIs for each phantom, yielding 384 (96 × 4) TSs in each ROI. The length of each TS was determined by the number of frames. TD, Spectral, and nonlinear features were computed and averaged within each ROI, providing a comprehensive analysis detailed in subsequent sections.

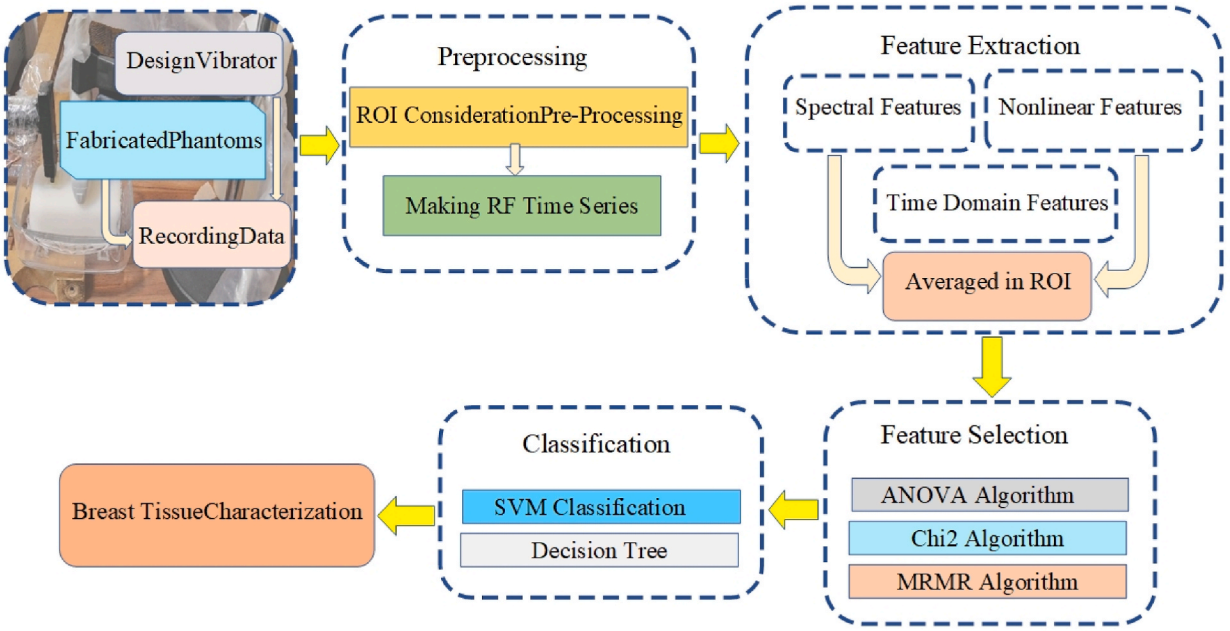

Fig. 3. General block diagram of the proposed method.

3.1.1. Time domain features

Spectral features have been recognized as the most impactful domain for analyzing RF time series [2,5,8,12–20]. In Refs. [12,17], wavelet features were also employed as time-frequency domain features; however, their results did not exhibit improvement compared to the spectral features introduced by Moradi et al. To facilitate a comprehensive comparison across time, spectral, and nonlinear domains, this paper also involves the extraction of 12 time features from each time series, subsequently averaging them within each ROI. These features include mean amplitude value (MAV), integrated absolute value (IAV), waveform length (WL), zero crossing (ZC), Willison amplitude (WA), slope sign change (SSC), variance (VAR), root mean square value (RMS), absolute value of the third, fourth, and fifth temporal moment (TRD, FRTH, and FFTH), and 4th order autoregressive coefficients (AR). For a detailed explanation of feature computation, readers are directed to Refs. [53,54].

3.1.2. Spectral features

The frequency-dependent characteristics of the returning wave phenomenon offer a valuable means to extract parameters and understand the propagation environment [55]. Employing the Fast Fourier Transform (FFT) as a compromise between time and frequency domain information, the research utilizes six parameters derived from the work of Moradi et al., summarizing the FFT-based power spectrum of RF TSs. These features involve averaging spectrum components over ROIs. Specifically, four features are obtained from the average values of the normalized spectrum in four quarters of the frequency range, and two additional features are determined from the slope and intercept of the regression line fitted to the magnitude of the frequency-normalized spectrum [19].

3.1.3. Nonlinear features

Biomedical signals, often nonlinear and apparently random, pose challenges for linear techniques like frequency domain analysis, which may not capture the complete spectrum [56,57]. This research recognizes the importance of nonlinear techniques in characterizing dynamic systems [58] and extracting 13 specific nonlinear features. Emphasis is placed on choosing nonlinear features well-suited for the TS analysis, particularly in the context of simulating tissue behavior using PVA phantoms. The results of all below-mentioned functions were averaged within each ROI and reported as nonlinear features.

Higuchi Fractal Dimension (HFD): Fractal Dimension (FD) serves as a valuable metric for assessing the internal dynamics' complexities within a TSs, as it determines scale-invariant roughness, even in non-fractal specimens, according to Mandelbrot. The need to prove the fractal nature of RF TS for FD calculations is deemed unnecessary for evaluating signal complexity [14]. Two approaches for FD estimation, operating in the time domain and the phase space, are highlighted [59]. The efficacy of HFD was suggested in RF TS for tissue typing [2,5,8,12–20]. This algorithm, designed for FD estimation in the time domain, establishes new TSs with interval times between successive points [58]. The application of Higuchi's algorithm involves decomposition with 10 and 16 levels for the TSs.

Hurst exponent: The Hurst exponent serves as a crucial metric for evaluating signal stability and instability within a dynamic system, directly tied to FD. Recognizing FD as the optimal feature for RF TS [2,5,8,12–20], our study systematically examined its relevance to our dataset. Various methods were considered for computing this parameter, with Detrended Fluctuation Analysis (DFA) identified as the primary technique for analyzing self-similarity in non-stationary TSs [58].

In DFA, the cumulative time series $y(t) = \sum_{i=1}^{t} x(i)$ is derived from the initial time series $x(t)$, which is divided into segments of length τ. For each segment, the fluctuation function, $F(\tau)$, is computed using the expression:

$$F^2(\tau) = \frac{1}{\tau} \sum_{t=1}^{\tau} (y(t) - Y_m(t))^2, \tag{1}$$

where $Y_m(t)$ represents a local m-polynomial trend within the segment [60]. The resulting averaged function $F(\tau)$ over the entire time series is proportional to τ^H:

$$F(\tau) \propto \tau^H, \tag{2}$$

where H denotes Hurst exponent. The generalized Hurst exponent (GHE) method is employed to directly analyze the scaling behavior of statistically significant variables constructed from the TSs. Various exponents associated with different characterizations of multi-scaling complexity are crucial for characterizing stochastic variables [61,62]. The parameter of a stochastic variable $X(t)$ is calculated using the following procedure:

$$K_q(\tau) = \langle |X(t+\tau) - X(t)|^q \rangle / \langle |X(t)|^q \rangle, \tag{3}$$

where the time interval τ varies between the time resolution and τ_{max}. The GHE $H(q)$ is defined by the scaling behavior of $K_q(\tau)$, assumed as:

$$K_q(\tau) \sim c\tau^{qH(q)}. \tag{4}$$

Utilizing different values of q representing distinct features, the mean and standard deviation of GHE for orders one to four were employed as eight features in our analysis.

Approximate entropy (ApEn): Introduced by Pincus in 1991, Approximate Entropy (ApEn) serves as a complexity measure for systems, especially valuable for limited finite sequences like the ultrafast mode TSs that are under consideration. ApEn stands out

among nonlinear dynamical methods, suitable for scenarios where entropy calculation is challenging, including chaotic and random signals, their combinations, and situations requiring stability against outlier data and noise reduction [58,59]. For ApEn calculation in a TS $x(n)$ with $n = 1,2...,N$, patterns of length e as the embedding dimension are considered, and ApEn is given by the formula:

$$ApEn(e,r,N) = \frac{1}{N-e+1}\sum_{i-1}^{N-e+1}\log C_i^e(r) - \frac{1}{N-e}\sum_{i-1}^{N-e}\log C_i^{e+1}(r), \tag{5}$$

where the index r is a fixed parameter that sets the tolerance of the comparison, and $C_i^e(r)$ denotes the correlation integral. The correlation integral is obtained as follows:

$$C_i^e(r) = \frac{1}{N-m+1}\sum_{j-1}^{N-e+1}\Theta\left(r - \left\|x_i - x_j\right\|\right), \tag{6}$$

where x_i and x_j represent trajectory points in the phase space, N is the number of data points in the phase space, r indicates the radial distance around each reference point, and Θ denotes the Heaviside function [63]. This algorithm was documented in Ref. [52] and used in this study.

Correlation dimension (CD): CD is a significant metric associated with the number of independent variables required to generate the degree of freedom, offering a means to quantify self-similarity. Various CD estimation methods, including Grassberger-Proccacia, Takens, Chord, and Ellner, have been proposed [64]. The algorithm for computation, based on the Grassberger-Proccacia estimator, is documented in Ref. [52], and we have employed this methodology in our analysis.

Lyapunov exponent (LE): LE serves as a quantifier for the average exponential rates of convergence or divergence of nearby phase space trajectories, providing insights into sensitivity to initial conditions. The LE algorithm, a well-established method employed in biomedical engineering, was first proposed by Wolf et al. in Ref. [65]. Different methods for computing the largest LE exist, and one of the practical and direct methods introduced by Rosenstein et al. [66] was utilized as the RF TS feature.

3.2. Classification

SVM is a well-established classifier for distinguishing between healthy and cancerous tissues, with proven success in previous studies [5,8,13–19] and our prior research [22,23]. Hence, the current investigation utilized the same group of classifiers, enabling a comparison of the results obtained from the proposed method with those reported in earlier studies. The SVM utilized five different kernels (Linear, Quadratic, Cubic, Fine Gaussian, and Medium Gaussian) for classifying each ROI. A 10-fold cross-validation method was applied at each step to ensure reliability and prevent overfitting [57]. The evaluation of the proposed system's performance encompassed seven parameters: accuracy, recall, specificity, precision or positive predictive value (PPV), negative predictive value (NPV), F score, and kappa which are defined as follows:

$$Accuracy = ((TP+TN)/(TP+FP+TN+FN)) \times 100, \tag{7}$$

$$Recall = ((TP)/(TP+FN)) \times 100, \tag{8}$$

$$Specificity = ((TN)/(TN+FP)) \times 100, \tag{9}$$

$$Precision = ((TP)/(TP+FP)) \times 100, \tag{10}$$

$$\mathrm{NPV} = ((TN)/(TN+FN)) \times 100, \tag{11}$$

$$F_{score} = ((2(Precision \times Sensitivity))/(Precision + Sensitivity)) \times 100, \tag{12}$$

where *TP, TN, FP,* and *FN* denote true positive, true negative, false positive, and false negative, respectively [67]. The kappa coefficient is an important index to evaluate the classification model [68]. Kappa can be calculated from a confusion matrix as:

$$kappa = ((Po - Pe)/(1 - Pe)) \times 100, \tag{13}$$

where *P*o and *P*e obtained from:

$$Po = ((TP+TN)/(TP+TN+FP+FN)). \tag{14}$$

$$Pe = ((TP+FN)\times(TP+FP) + (FP+TN)\times(FN+TN))\Big/(TP+TN+FP+FN)^2. \tag{15}$$

Furthermore, Random Forest, along with three sets of decision tree classifiers (Fine, Medium, and Course decision trees), was incorporated to enhance the comparative analysis. A 10-fold cross-validation was performed at each step, and 12 complete repetitions of each classification were employed to ensure robust evaluation.

4. Results

In this section, we present the results organized into three subgroups. In 4.1, we have thoroughly examined three domain features and reported the average performance of classifiers for each type of data. Following this, we have utilized feature selection algorithms to identify the most effective feature group. The results of this optimal feature group for classifying different types of data are detailed in Table 2. In 4.2, we have investigated three different groups of machine learning for classifying various types of data and stimulation. In the final segment, we have scrutinized evaluation parameters of our top-performing classifier group, SVM, across different stimulations. We have evaluated the robustness of these results not only through the k-fold method but also via the holdout method.

4.1. TD, spectral, and nonlinear features in classification

The study aimed to identify the most effective feature for classifying four types of tissues by employing 12 TD, six spectral, and 13 nonlinear features independently and in combination. The outcomes averaged across five SVM classifiers, are presented in graphs for three distinct groups of data, each representing six types of stimulations. These stimulations included simple mode, static mode (when a constant force was applied to the tissue), and vibrational mode. The effectiveness of vibration displacements on the RF backscattering patterns was assessed by allowing vibrations to spread throughout the tissue at frequencies of 35, 45, 55, and 65 Hz and then recording RF data. The mean classification accuracies of the SVMs, averaged across six types of stimulations, are illustrated in Fig. 4, and the error bars denote the standard deviation after 12 repetitions of each complete classification.

The optimal outcome, in terms of mean accuracy, was observed for five SVM kernels within the context of beamformed ultrafast data, leveraging both spectral and nonlinear features. While TD and spectral features demonstrated satisfactory performance in classifying raw focused data, the inclusion of nonlinear features proved highly effective for other data types. Furthermore, in addition to this comparison, feature selection was explored using ANOVA, Chi2, and MRMR algorithms. The mean scores of these algorithms are illustrated in Fig. 5 for six types of stimulations considering the beamformed ultrafast data.

Due to variations in algorithmic scores across all 18 groups of data, a set of 19 features was consistently applied to the entire dataset. The mean values for seven evaluation parameters, computed across five SVM classifiers, are detailed in Table 2. Each data mode was further categorized into three distinct stimulations, with the term "vibration" denoting the averaged results from four different states of vibrator usage. All outcomes are presented as mean ± SD% which were reported after 12 repetitions of each complete classification, ensuring more robust testing of machine learning results and comprehensive evaluation. The expression of the classification results by separating the type of stimulation, showed that RFTSDP and ultrafast data can improve tissue classification.

4.2. Classification evaluation of different machine learning models

It should be noted that in vibrational stimulation, the vibration frequency significantly affects the improvement of classification accuracy. Therefore, in the following sections, the vibrating frequencies have been investigated separately. The accuracy of Random Forest, as well as the mean accuracy of decision trees and SVMs, are compared in Fig. 6.

The reported results pertain to beamformed ultrafast data, which exhibited the highest SVM classification accuracy. As depicted in Fig. 6, SVM outperformed decision trees and Random Forest across all stimulation types when considering beamformed ultrafast data, except for the simple type.

Table 2
Mean results of Linear, Quadratic, Cubic, Fine Gaussian, and Medium Gaussian SVM in time series of raw focused, raw, and beamformed ultrafast data.

Data Mode	Stimulation type	Mean Accuracy(%)	Mean Kappa(%)	Mean Precision(%)	*Mean NPV (%)*	Mean Specificity(%)	Mean F1score(%)	Mean Recall(%)
Raw Focused	*Simple*	77.12 ± 1.69	69.76 ± 2.16	78.26 ± 1.52	92.44 ± 0.58	92.40 ± 0.56	77.31 ± 1.59	77.21 ± 1.69
	Static	63.80 ± 2.19	50.54 ± 2.93	61.87 ± 2.51	88.31 ± 0.75	87.93 ± 0.73	62.34 ± 2.19	63.80 ± 2.19
	Vibration	77.47 ± 2.01	70.40 ± 2.47	79.47 ± 1.71	92.47 ± 0.70	92.49 ± 0.67	77.92 + 1.87	77.47 + 2.01
Raw Ultrafast	*Simple*	89.19 ± 1.41	85.55 ± 1.85	89.77 ± 1.55	96.47 ± 0.49	96.39 ± 0.47	89.14 ± 1.38	89.19 ± 1.41
	Static	91.20 ± 1.22	88.26 ± 1.67	91.78 ± 1.31	97.03 ± 0.39	97.06 ± 0.40	91.14 ± 1.27	91.21 ± 1.20
	Vibration	93.23 ± 2.77	90.81 ± 1.61	93.33 ± 2.08	97.81 ± 0.67	97.74 ± 0.66	93.07 ± 1.98	93.23 + 1.94
Beamformed Ultrafast	*Simple*	94.14 ± 1.65	92.25 ± 2.17	94.64 ± 1.75	98.07 ± 0.57	98.05 ± 0.55	94.21 ± 1.62	94.14 ± 1.65
	Static	96.87 ± 0.00	95.78 ± 0.00	96.61 ± 0.47	99.00 ± 0.00	98.75 ± 0.00	96.82 ± 0.00	95.35 ± 0.00
	Vibration	97.35 ± 0.67	95.93 ± 0.87	97.06 ± 0.01	98.81 ± 0.55	98.93 ± 0.22	96.35 ± 0.66	96.87 ± 0.67

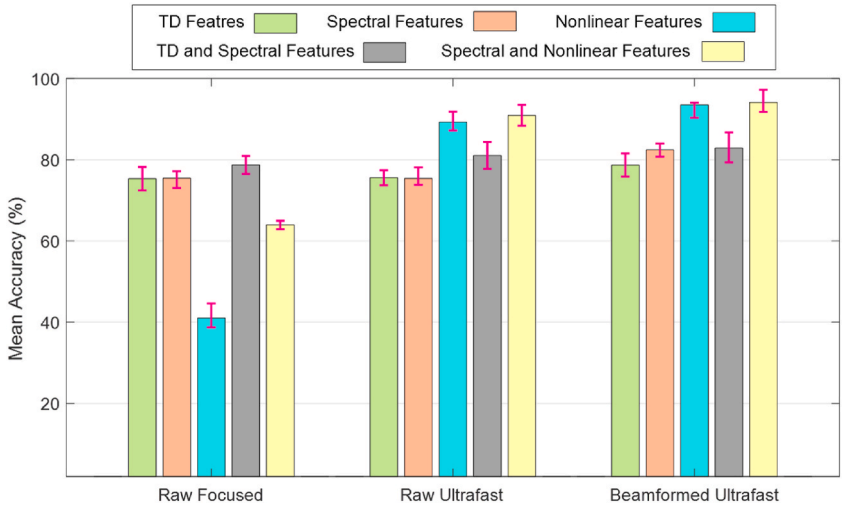

Fig. 4. Mean accuracy (%) of Linear, Quadratic, Cubic, Fine Gaussian, and Medium Gaussian SVM for three stimulation types of raw focused data, raw ultrafast data, and beamformed ultrafast data. The error bars represent the standard deviation calculated from 12 repetitions of each complete classification.

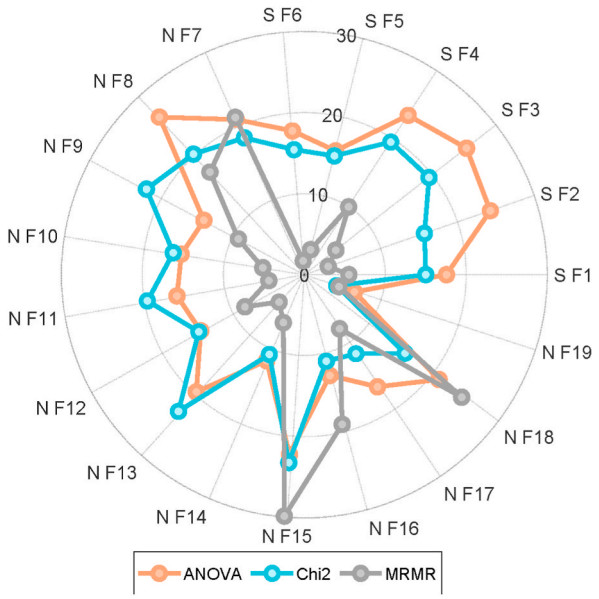

Fig. 5. Mean scores of feature selection ANOVA, Chi2, and MRMR algorithms in beamformed ultrafast data. SF means spectral feature and NF means nonlinear feature. SF1 to SF4 is related to the average values of the normalized spectrum in four quarters of the frequency range; SF5 and SF6 are the slope and intercept of the regression line. NF7 represents HFD, NF8 is Hurst exponent (DFA analysis), NF9 to NF16 are the mean and standard deviation of the GHE with q = 1,2,3,4, NF17 is ApEn, NF18 is LE, and NF19 represents CD.

4.3. Evaluation of SVM performance in vibrational stimulations

To provide a comprehensive evaluation of this classifier, additional parameters were computed in this mode. The average of seven evaluation parameters for five SVM classifiers in beamformed ultrafast data, encompassing all types of vibrational stimulations, is illustrated in Fig. 7. The error bars represent the standard deviation calculated from 12 repetitions of each complete classification. This approach facilitates a thorough examination and comparison of vibrational stimulation at different frequencies.

The training and testing of machine learning models should be assessed with a robust procedure to determine if the models are producing overoptimistic accuracy estimations [69]. To accomplish this, a portion of the training data is withheld for testing purposes, mimicking scenarios that commonly occur in clinical studies. Specifically, SVMs are trained while holding out 10 %, 30 %, 50 %, and 70 % of the data for testing.

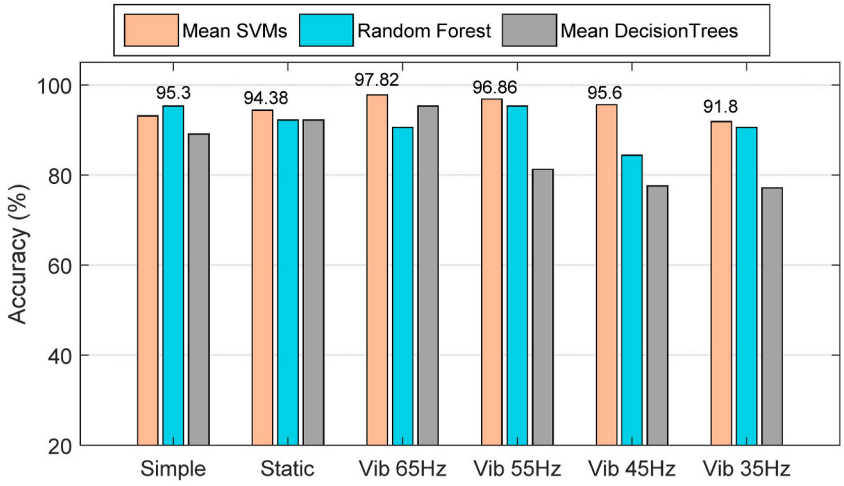

Fig. 6. The accuracy of Random Forest and mean accuracy of Fine, Medium, and Course decision trees and five kernels of SVM in the classification of TSs constructed from beamformed ultrafast data. Vib 65Hz means vibration at 65 Hz.

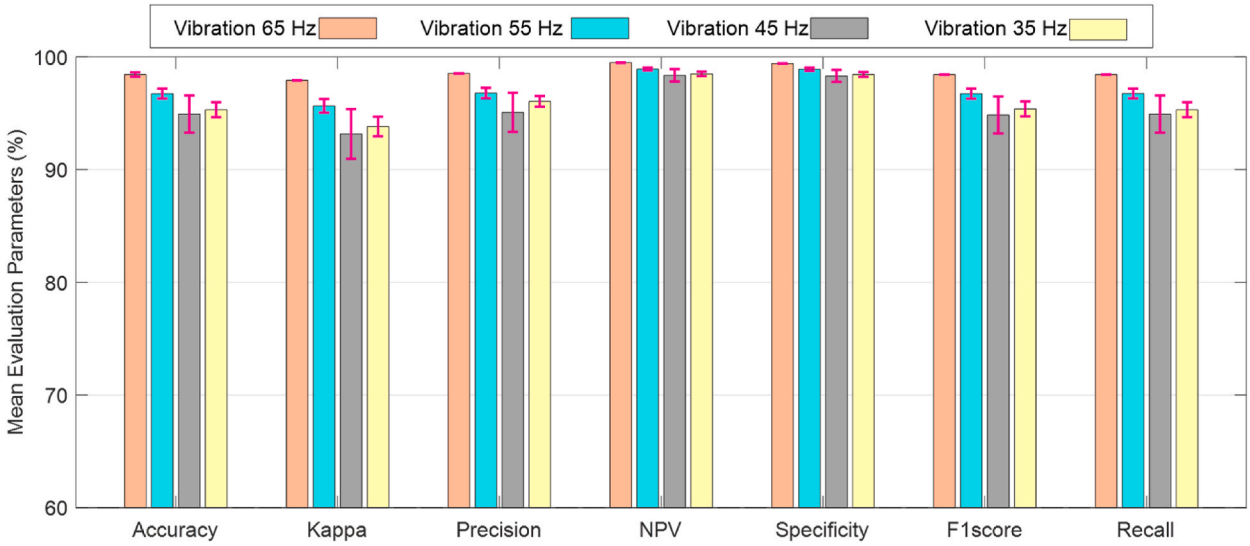

Fig. 7. Mean results of Linear, Quadratic, Cubic, Fine Gaussian, and Medium Gaussian SVM achieved for TSs of beamformed ultrafast data. The error bars represent the standard deviation calculated from 12 repetitions of each complete classification.

Mean evaluation parameters for five SVM classifiers, encompassing 65 Hz vibrational stimulation in beamformed ultrafast data (our best result), are depicted in Fig. 8 using this methodology. The error bars represent the standard deviation calculated from 12 repetitions of each complete classification.

5. Discussion

The relationship between tissue elasticity and pathological processes underscores the potential for more accurate lesion diagnosis based on elastic coefficients. Studies in elastography, such as [70], have demonstrated changes in return signal patterns caused by applied tissue surface vibration. Vibro-elastography and transient elastography utilize this signal information to estimate elasticity by determining displacement. Recent studies have explored nonlinear models to capture tissue's dynamic and nonlinear behavior. However, these models require complex calculations and may only represent a portion of tissue behavior. A more recent and promising approach involves examining the RF signals and the resulting TSs in US-based methods.

We proposed the combination of these two methods in RFTSDP. In this method, the RF TS is investigated while applying different tissue stimulation. Thus, information related to the mechanical and elastic properties of the tissue can be encoded in the output signal. By processing this signal and extracting the appropriate features, tissue classification results can be improved. We made four different

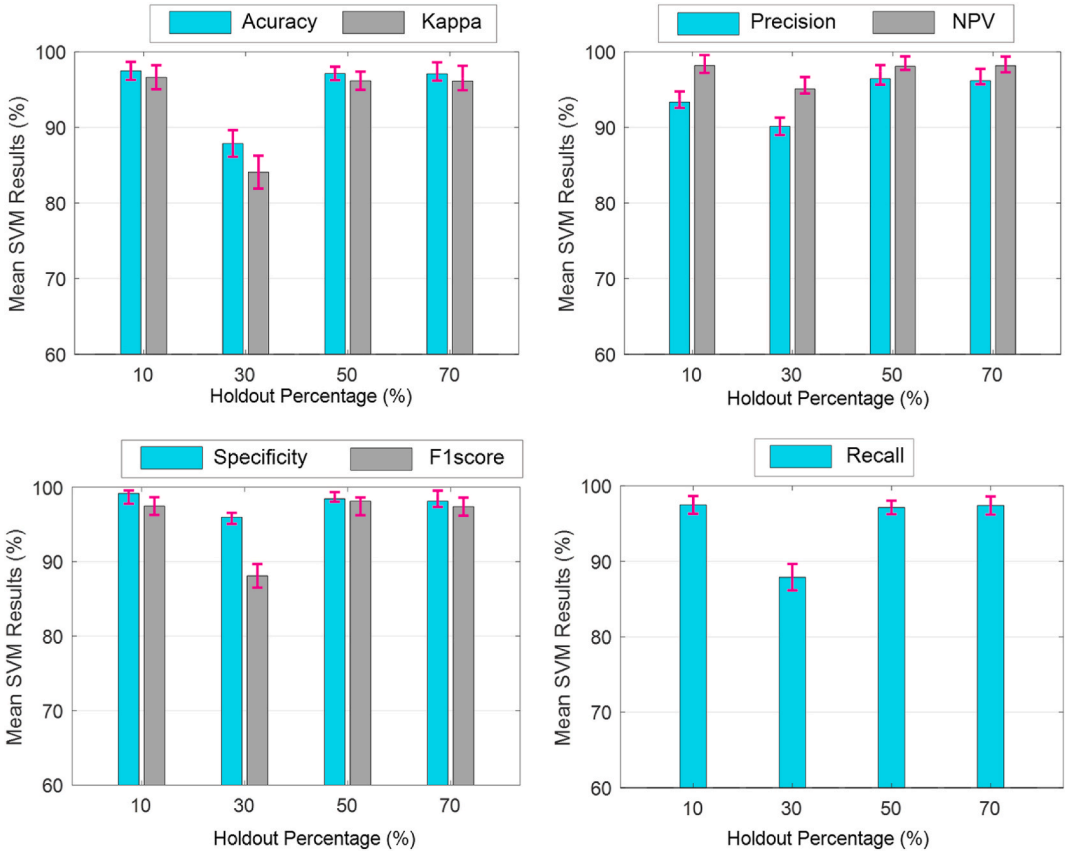

Fig. 8. Mean results of Linear, Quadratic, Cubic, Fine Gaussian, and Medium Gaussian SVM achieved for TSs of beamformed ultrafast data. The error bars represent the standard deviation calculated from 12 repetitions of each complete classification.

PVA-based breast phantoms (i.e., healthy tissue and lesions) to achieve the best way of characterization of acoustic and mechanical properties.

For a more in-depth look at this method and to determine the effect of tissue stimulation on the RF echo, several types of stimulation

Table 3
Comparison of relevant RF time series methods.

Research	Data	Feature Extraction	Classifier	No. of classes	Accuracy (%)
Uniyal et al. [2]	British Columbia University dataset (22 subjects)	• Spectral Features • HFD • Textural B-mode Features	SVM Random Forest	2	86 81
Moradi et al. [8]	Extracted Prostate	• Statistical B-mode Image Features • HFD	Neural Networks	2	95.40
Aboofazeli et al. [12]	35 Extracted Prostates	• Wavelet Transform • Spectral Features • HFD	SVM	2	91.70
Moradi et al. [19]	Agar-Gelatin Phantoms	• Spectral Features • HFD	SVM	2	82.20
Imani et al. [16,17]	7-14 in-vivo Subject	• Wavelet Transform • Spectral Feature	SVM	2	80
Moradi et al. [14]	Animal Tissues	• Spectral Features • HFD	SVM	2 4	95.10 78.60
Jarosik et al. [33]	OASBUD (78 subjects and 100 RF Data)	• Deep Learning	CNN	2	70.10
Ghehi et al. [22,23]	Agar-Gelatin Phantom	• Spectral Features • HFD	SVM	2	98.78
Proposed RFTSDP Method	PVA Phantoms	• Spectral Features • Nonlinear Features	SVM Random Forest Decision tree	4	97.82 90.60 95.30

were considered. A vibrator was designed, made, and used for recording data in three types of stimulation. It should be noticed that the vibration frequency was in the range of tissue dynamic response.

Using two groups of features separately in Fig. 4, showed that TD and spectral features were more useful than nonlinear features in raw focused data classification. However, the opposite result was observed in raw and beamformed ultrafast data. By implementing the nonlinear features, 18.45 % and 13.44 % improvements were achieved in raw and beamformed ultrafast data classification accuracy, respectively. The best result was related to the combination of features in beamformed ultrafast data with 94.13 % accuracy averaged across different types of stimulation. All results were the mean results of five SVM classifiers mentioned in the previous section.

According to the results, in RFTSDP, it would be better to investigate the nonlinear characterization of RF TS in ultrafast data. The ultrafast mode provides the possibility of tracking the effect of stimulation on the pattern of scatterers. Considering the appearance of tissue dynamic response to the applied stimulation, the 23.99 % improvement in mean accuracy can be justified by using nonlinear features and beamformed ultrafast data compared to TD and spectral features in focused data.

A more detailed investigation of the features was conducted on the beamformed ultrafast data. ANOVA, Chi2, and MRMR algorithms were employed for feature selection (refer to Fig. 5). Using the Chi2 algorithm, a score near zero was assigned to all spectral features and some nonlinear features. Meanwhile, the ANOVA and MRMR algorithms yielded similar scores for spectral and nonlinear features. Based on the results of these algorithms for all data, it was ultimately decided to utilize all 19 features in the continuation of this work.

The mean of seven evaluation parameters in four-class SVMs, are presented in Table 2. The results were reported based on the type of stimulation for all three data modes. This approach allowed for a clear determination of the effect of the stimulation type and the proposed method on improving classification performance. It was observed that in all data modes, there was an improvement in accuracy achieved by applying vibration compared to the simple mode. The best result was associated with the beamformed ultrafast data in vibrational mode. The average accuracy and precision attained for recordings at different frequencies of vibration were 97.35 ± 0.67 % and 97.06 ± 0.01 %, respectively. Additionally, this mode exhibited a 34.99 % accuracy improvement compared to the simple mode when using focused raw data. A summary of some tissue classification and tissue typing results in RF field research is provided in Table 3.

Since investigations in most of Moradi's team research were conducted on agar-gelatin phantoms or prostate tissue in two healthy and cancerous groups, making an exact comparison is not feasible. The TSs in the simple mode were utilized to classify four different animal tissues [14]. In these four-class classification experiments, the accuracy reached 78.6 % with a 6.6 MHz probe central frequency.

The classification parameters for vibration stimulation with different frequencies were reported separately in Fig. 6. The best result was observed for vibration at 65 Hz frequency in beamformed ultrafast data. In this case, the classification accuracy and precision were 98.44 % and 98.53 %, respectively. Therefore, in RFTSDP, applying appropriate vibration compared to the simple mode in beamformed ultrafast data led to a 5.02 % improvement in accuracy, and compared to the results of four-class tissue typing in Ref. [14], a 24.45 % improvement in accuracy was achieved.

To compare the performance of the classifier, besides SVMs, Random Forest, different types of KNN, and decision trees were also employed. The KNNs exhibited very low accuracy in this four-class classification. The accuracy of Random Forest and mean results of decision trees, which were comparable to SVM for ultrafast beamformed data, are depicted in Fig. 5. For a more detailed analysis, the mean accuracy for all types of stimulation was reported separately. In all cases, the four-class SVM outperformed the decision trees.

In conclusion, among the stimulations applied, including stimulation with constant force and vibration at various frequencies, vibration, especially at 65 Hz, significantly influenced classification outcomes. The vibration caused the displacement of phantom scatterers, leading to alterations in RF backscattering patterns and subsequent improvements in classification results. Additionally, it was observed that for studying RF TS under vibration, sampling the data at high speed is preferable to track the effects of vibration on return patterns and scatterers' displacements, thereby providing deeper insights into the dynamics of the environment during tissue vibration. The findings presented in this paper highlight that the best classification performance was achieved by employing appropriate vibration in the ultrafast mode.

Furthermore, the optimal classification results for three types of breast lesions and healthy tissue were observed in the beamformed ultrafast data, as anticipated due to its higher imaging speed and superior ability to track movement. Moreover, across all types of stimulation, the most favorable outcomes were obtained by utilizing 19 spectral and nonlinear features in conjunction with 65 Hz vibration, resulting in accuracy and precision levels of 97.82 % and 99.27 %, respectively. Thus, vibration can provide valuable insights into TSs, particularly in beamformed ultrafast data.

Our models were also tested by the approach of holdout, withholding 10 %, 30 %, 50 %, and 70 % of the data for the testing phase. We implemented this to assess the robustness of the selected features for training classifiers when limited training data are available, as often occurs in clinical experiments. The results in Fig. 8 indicate consistent classification performance across all parameters, except for a significant drop observed at 30 % holdout, including a reduction in training data adversely affecting performance.

The appropriate frequency for vibration depends on various factors, including the type of tissue, recording conditions, center frequency of the probe, and US imaging mode. As the results demonstrate, the classifier exhibits weaker performance at certain vibration frequencies. Since RF echo signals are frequency-dependent, identifying the optimal vibration frequency and extracting suitable features based on recording conditions are crucial. The study concludes that combining spectral and non-linear features was more effective for characterization.

The study presents several limitations that warrant consideration. The investigative process, particularly in methodologies like elastography that involve external stimulation, typically follows a systematic sequence. This involves initial scrutiny using a phantom, followed by examinations on animal or ex-vivo human tissues, and eventually culminating in in-vivo investigations, mirroring the

approach employed in numerous longitudinal studies discussed in the literature review.

While the current study aimed to utilize optimal tissue-mimicking materials for phantom construction, it is important to acknowledge that the resulting phantoms were uniformly constructed. This uniformity poses a limitation to the study, as exploring the intricacies of different breast tissues and the lesion environment together could have provided a more comprehensive understanding. Despite the meticulous selection of materials, the inherent constraint of studying solely on phantoms must be recognized.

Future research endeavors might benefit from utilizing different tissue phantom compositions or ex-vivo tissue in normal tissue phantoms to enhance the generalizability and robustness of findings, and better evaluate the novel RFTSDP method in the natural environment.

In our experimental setup, we employed the same US recording equipment, which also allows for the investigation of raw RF echo and has an ultrafast mode for better tracking of backscatter movements. To implement the proposed idea in RFTSDP, only one vibrator was utilized, as referenced in the methods section. The vibrator was positioned two cm from the probe on the medium surface, potentially influencing the US probe. Additionally, for effective utilization of this method, the designed vibrator must be more accurate and controllable regarding the applied force and frequency generated within the targeted tissue. This aspect is also under investigation by our elastography group. For the future advancement of the RFTSDP method, designing a suitable vibrator that minimally affects the probe should be considered. This vibrator, after the mentioned enhancements, can easily be used alongside the US probe for clinical recordings.

Apart from spectral features, we innovatively incorporated nonlinear features to better discern the dynamic behavior of tissues. While considering the exploration of more nonlinear features or the application of deep learning with a richer database, we refrained from employing deep learning due to the limited dataset in this study. Notably, existing research highlights the challenge of improving deep learning models with limited datasets [3]. Despite its potential, deep learning suffers from drawbacks such as high computational costs, interpretability issues, data quality dependence, unforeseen consequences, and the opaque nature of black-box models [71]. The study also suggests future investigation of RFTSDP using deep learning methods to automatically extract efficacious features and enhance ex-vivo and in-vivo breast lesion classification.

6. Conclusions

In this paper, we aimed to investigate RF TSs while applying external stimulation to tissues, thereby incorporating dynamic tissue properties into the information recorded by the RF signal. We compared the results of the proposed dynamic stimulation approach, called RFTSDP, with relevant techniques, specifically one suggested by Moradi et al. [8], where the probe and tissue were fixed. By utilizing a simple vibrator with varying frequencies, we found that a vibration frequency of 65 Hz yielded the highest classification accuracy across all data types. The outcomes of this study confirmed that integrating RF TS analysis with dynamic tissue stimulation enriches RF signal information for tissue typing and improves the classification accuracy of breast lesions.

It is imperative to direct the study of the proposed idea in this paper and the introduced method, RFTSDP, towards the utilization of ex-vivo tissue samples and ultimately examine it in-vivo. We look forward to carrying out clinical studies that involve large samples from various types of both cancerous and noncancerous breast lesions.

Data availability statement

Our data for these four phantoms, including raw focused data, raw and beamformed ultrafast data for all the stimulations mentioned in this paper and our previous studies, can be requested from the following address: *http://elastography.ir*.

CRediT authorship contribution statement

Elaheh Norouzi Ghehi: Writing – review & editing, Writing – original draft, Visualization, Validation, Software, Resources, Methodology, Investigation, Formal analysis, Data curation, Conceptualization. **Ali Fallah:** Writing – review & editing, Validation, Supervision, Project administration, Methodology, Formal analysis, Data curation, Conceptualization. **Saeid Rashidi:** Writing – review & editing, Validation, Supervision, Project administration, Methodology, Formal analysis, Data curation, Conceptualization. **Maryam Mehdizadeh Dastjerdi:** Writing – review & editing, Validation, Supervision, Software, Project administration, Methodology, Formal analysis, Data curation, Conceptualization.

Declaration of competing interest

The authors declare that they have no known competing financial interests or personal relationships that could have appeared to influence the work reported in this paper.

Acknowledgments

The authors would like to express their gratitude to all the researchers whose articles were utilized in this research. They also appreciate Dr. S. Ghasemirad (Department of Polymer Engineering, Tarbiat Modares University, Tehran, Iran) for her inspiring advice in fabricating PVA phantoms, and the manager, Eng. Reza Rashidzadeh, and the employees of Tanasa Teb Novin Company, Tehran, Iran, for providing us with the Supersonic Imaging Axiplorer US system.

References

[1] P. Song, et al., Diagnostic performance of ultrasound with computer-aided diagnostic system in detecting breast cancer, Heliyon 9 (10) (2023) e20712, https://doi.org/10.1016/j.heliyon.2023.e20712.
[2] N. Uniyal, et al., Ultrasound RF time series for classification of breast lesions, IEEE Trans. Med. Imag. 34 (2) (2014) 652–661, https://doi.org/10.1109/TMI.2014.2365030.
[3] R.A. Dar, M. Rasool, A. Assad, Breast cancer detection using deep learning: datasets, methods, and challenges ahead, Comput. Biol. Med. (2022) 106073, https://doi.org/10.1016/j.compbiomed.2022.106073.
[4] A. Godavarty, et al., Optical imaging for breast cancer prescreening, Breast Cancer (2015) 193–209.
[5] M. Moradi, et al., A new approach to analysis of RF ultrasound echo signals for tissue characterization: animal studies, in: Medical Imaging 2007: Ultrasonic Imaging and Signal Processing, 2007, https://doi.org/10.1117/12.708630. SPIE.
[6] W. Wang, et al., Strain estimation by a Fourier Series-based extrema tracking algorithm for elastography, Ultrasonics 62 (2015) 278–291, https://doi.org/10.1016/j.ultras.2015.05.028.
[7] P. Martins, R. Natal Jorge, A. Ferreira, A comparative study of several material models for prediction of hyperelastic properties: application to silicone-rubber and soft tissues, Strain 42 (3) (2006) 135–147, https://doi.org/10.1111/j.1475-1305.2006.00257.x.
[8] M. Moradi, et al., Detection of prostate cancer from RF ultrasound echo signals using fractal analysis, in: 2006 International Conference of the IEEE Engineering in Medicine and Biology Society, IEEE, 2006.
[9] S. Golemati, D.D. Cokkinos, Recent advances in vascular ultrasound imaging technology and their clinical implications, Ultrasonics 119 (2022) 106599, https://doi.org/10.1016/j.ultras.2021.106599.
[10] J.R. Doherty, et al., Acoustic radiation force elasticity imaging in diagnostic ultrasound, IEEE Trans. Ultrason. Ferroelectrics Freq. Control 60 (4) (2013) 685–701, https://doi.org/10.2174/157340511798038657.
[11] C. Liu, et al., Quantitative characterization of the colorectal cancer in a rabbit model using high-frequency endoscopic ultrasound, Ultrasonics 110 (2021) 106289, https://doi.org/10.1016/j.ultras.2020.106289.
[12] M. Aboofazeli, et al., Automated detection of prostate cancer using wavelet transform features of ultrasound RF time series, in: Medical Imaging 2009: Computer-Aided Diagnosis, 2009, https://doi.org/10.1117/12.813831. SPIE.
[13] M. Moradi, et al., Augmenting detection of prostate cancer in transrectal ultrasound images using SVM and RF time series, IEEE (Inst. Electr. Electron. Eng.) Trans. Biomed. Eng. 56 (9) (2008) 2214–2224, https://doi.org/10.1109/TBME.2008.2009766.
[14] M. Moradi, P. Abolmaesumi, P. Mousavi, Tissue typing using ultrasound RF time series: experiments with animal tissue samples, Med. Phys. 37 (8) (2010) 4401–4413, https://doi.org/10.1118/1.3457710.
[15] S.S. Mahdavi, et al., Evaluation of visualization of the prostate gland in vibro-elastography images, Med. Image Anal. 15 (4) (2011) 589–600, https://doi.org/10.1016/j.media.2011.03.004.
[16] F. Imani, et al., Ultrasound-based characterization of prostate cancer: an in vivo clinical feasibility study, in: Medical Image Computing and Computer-Assisted Intervention–MICCAI 2013: 16th International Conference, Nagoya, Japan, September 22-26, 2013, Proceedings, Part II 16, Springer, 2013.
[17] F. Imani, et al., Computer-aided prostate cancer detection using ultrasound RF time series: in vivo feasibility study, IEEE Trans. Med. Imag. 34 (11) (2015) 2248–2257, https://doi.org/10.1109/TBME.2015.2404300.
[18] A. Khojaste, et al., Characterization of aggressive prostate cancer using ultrasound RF time series, in: Medical Imaging 2015: Computer-Aided Diagnosis, 2015, https://doi.org/10.1117/12.2082663. SPIE.
[19] M. Moradi, et al., Tissue typing with ultrasound RF time series: phantom studies, in: Medical Imaging 2009: Ultrasonic Imaging and Signal Processing, 2009, https://doi.org/10.1117/12.811693. SPIE.
[20] M. Moradi, et al., P6C-7 ultrasound RF time series for detection of prostate cancer: feature selection and frame rate analysis, in: 2007 IEEE Ultrasonics Symposium Proceedings, IEEE, 2007, https://doi.org/10.1109/ULTSYM.2007.627.
[21] M. Brock, et al., Multiparametric ultrasound of the prostate: adding contrast enhanced ultrasound to real-time elastography to detect histopathologically confirmed cancer, J. Urol. 189 (1) (2013) 93–98, https://doi.org/10.1016/j.juro.2012.08.183.
[22] E.N. Ghehi, et al., Effect of tissue excitation in breast cancer detection from ultrasound RF time series: phantom studies, in: 2021 11th International Conference on Computer Engineering and Knowledge (ICCKE), IEEE, 2021, https://doi.org/10.1109/ICCKE54056.2021.9721530.
[23] E.N. Ghehi, et al., Breast cancer detection from a new ultrasound RF time series based approach: phantom studies, in: 2021 28th National and 6th International Iranian Conference on Biomedical Engineering (ICBME), IEEE, 2021, https://doi.org/10.1109/ICBME54433.2021.9750306.
[24] C.-Y. Lin, et al., Early detection and assessment of liver fibrosis by using ultrasound RF time series, J. Med. Biol. Eng. 37 (2017) 717–729.
[25] Q. Lin, et al., Ultrasonic RF time series for early assessment of the tumor response to chemotherapy, Oncotarget 9 (2) (2018) 2668, https://doi.org/10.1109/JBHI.2021.3103676.
[26] M.M. Monfared, et al., High-intensity focused ultrasound thermal lesion detection using entropy imaging of ultrasound radio frequency signal time series, J. Med. Ultrasound 26 (1) (2018) 24, https://doi.org/10.4103/JMU.JMU_3_17.
[27] S. Mobasheri, et al., Radio frequency ultrasound time series signal analysis to evaluate high-intensity focused ultrasound lesion formation status in tissue, Journal of medical signals and sensors 6 (2) (2016) 91.
[28] A. Behnia, et al., Thermometry using entropy imaging of ultrasound radio frequency signal time series, Proc. IME H J. Eng. Med. 236 (10) (2022) 1502–1512, https://doi.org/10.1177/09544119221122645.
[29] M.F. Ak, A comparative analysis of breast cancer detection and diagnosis using data visualization and machine learning applications, in: Healthcare, MDPI, 2020, https://doi.org/10.3390/healthcare8020111.
[30] S. Muhtadi, Breast tumor classification using intratumoral quantitative ultrasound descriptors, Comput. Math. Methods Med. (2022), https://doi.org/10.1155/2022/1633858, 2022.
[31] Y. Shao, et al., Breast cancer detection using multimodal time series features from ultrasound shear wave absolute vibro-elastography, IEEE Journal of Biomedical and Health Informatics 26 (2) (2021) 704–714.
[32] B. Behboodi, et al., Deep classification of breast cancer in ultrasound images: more classes, better results with multi-task learning, in: Medical Imaging 2021: Ultrasonic Imaging and Tomography, 2021, https://doi.org/10.1117/12.2581930. SPIE.
[33] P. Jarosik, et al., Breast lesion classification based on ultrasonic radio-frequency signals using convolutional neural networks, Biocybern. Biomed. Eng. 40 (3) (2020) 977–986, https://doi.org/10.1016/j.bbe.2020.04.002.
[34] M. Qiao, et al., Breast calcification detection based on multichannel radiofrequency signals via a unified deep learning framework, Expert Syst. Appl. 168 (2021) 114218, https://doi.org/10.1016/j.eswa.2020.114218.
[35] M. Byra, et al., Joint segmentation and classification of breast masses based on ultrasound radio-frequency data and convolutional neural networks, Ultrasonics 121 (2022) 106682, https://doi.org/10.1016/j.ultras.2021.106682.
[36] G.R. Gare, et al., W-Net: dense and diagnostic semantic segmentation of subcutaneous and breast tissue in ultrasound images by incorporating ultrasound RF waveform data, Med. Image Anal. 76 (2022) 102326, https://doi.org/10.1016/j.media.2021.102326.
[37] D. Painuli, S. Bhardwaj, Recent advancement in cancer diagnosis using machine learning and deep learning techniques: a comprehensive review, Comput. Biol. Med. 146 (2022) 105580, https://doi.org/10.1016/j.compbiomed.2022.105580.
[38] A. Chowdhury, et al., Ultrasound classification of breast masses using a comprehensive Nakagami imaging and machine learning framework, Ultrasonics 124 (2022) 106744, https://doi.org/10.1016/j.ultras.2022.106744.
[39] S. Hossain, et al., Automated breast tumor ultrasound image segmentation with hybrid UNet and classification using fine-tuned CNN model, Heliyon 9 (11) (2023) e21369.

[40] M. Alotaibi, et al., Breast cancer classification based on convolutional neural network and image fusion approaches using ultrasound images, Heliyon 9 (11) (2023) e22406, https://doi.org/10.1016/j.heliyon.2023.e22406.
[41] K. Manickam, R.R. Machireddy, S. Seshadri, Characterization of biomechanical properties of agar based tissue mimicking phantoms for ultrasound stiffness imaging techniques, J. Mech. Behav. Biomed. Mater. 35 (2014) 132–143, https://doi.org/10.1016/j.jmbbm.2014.03.017.
[42] H. Mehrabian, A. Samani, Constrained hyperelastic parameters reconstruction of PVA (Polyvinyl Alcohol) phantom undergoing large deformation, in: Medical Imaging 2009: Visualization, Image-Guided Procedures, and Modeling, 2009, https://doi.org/10.1117/12.813871. SPIE.
[43] K. Zell, et al., Acoustical properties of selected tissue phantom materials for ultrasound imaging, Phys. Med. Biol. 52 (20) (2007) N475, https://doi.org/10.1088/0031-9155/52/20/N02.
[44] A. Kharine, et al., Poly (vinyl alcohol) gels for use as tissue phantoms in photoacoustic mammography, Phys. Med. Biol. 48 (3) (2003) 357, https://doi.org/10.1088/0031-9155/48/3/306.
[45] H. Mehrabian, G. Campbell, A. Samani, A constrained reconstruction technique of hyperelasticity parameters for breast cancer assessment, Phys. Med. Biol. 55 (24) (2010) 7489, https://doi.org/10.1088/0031-9155/55/24/007.
[46] C.U. Devi, R.M. Vasu, A. Sood, Design, fabrication, and characterization of a tissue-equivalent phantom for optical elastography, J. Biomed. Opt. 10 (4) (2005), https://doi.org/10.1117/1.2003833, 044020-044020-10.
[47] S. Jiang, S. Liu, W. Feng, PVA hydrogel properties for biomedical application, J. Mech. Behav. Biomed. Mater. 4 (7) (2011) 1228–1233, https://doi.org/10.1016/j.jmbbm.2011.04.005.
[48] L. Braunstein, et al., Characterization of acoustic, cavitation, and thermal properties of poly (vinyl alcohol) hydrogels for use as therapeutic ultrasound tissue mimics, Ultrasound Med. Biol. 48 (6) (2022) 1095–1109, https://doi.org/10.1016/j.ultrasmedbio.2022.02.007.
[49] W. Xia, et al., Poly (vinyl alcohol) gels as photoacoustic breast phantoms revisited, J. Biomed. Opt. 16 (7) (2011), https://doi.org/10.1117/1.3597616, 075002-075002-10.
[50] A. Samani, J. Zubovits, D. Plewes, Elastic moduli of normal and pathological human breast tissues: an inversion-technique-based investigation of 169 samples, Phys. Med. Biol. 52 (6) (2007) 1565, https://doi.org/10.1088/0031-9155/52/6/002.
[51] J. Fromageau, et al., Estimation of polyvinyl alcohol cryogel mechanical properties with four ultrasound elastography methods and comparison with gold standard testings, IEEE Trans. Ultrason. Ferroelectrics Freq. Control 54 (3) (2007) 498–509.
[52] MathWorks, MATLAB 2022b. Natick, MA: MathWorks, Available from: https://www.mathworks.com/products/matlab.html, 2022.
[53] A. Mengarelli, et al., Identification of neurodegenerative diseases from gait rhythm through time domain and time-dependent spectral descriptors, IEEE Journal of Biomedical and Health Informatics 26 (12) (2022) 5974–5982.
[54] A. Phinyomark, et al., EMG feature evaluation for improving myoelectric pattern recognition robustness, Expert Syst. Appl. 40 (12) (2013) 4832–4840, https://doi.org/10.1016/j.eswa.2013.02.023.
[55] E. Dehghan-Niri, H. Al-Beer, Phase-space topography characterization of nonlinear ultrasound waveforms, Ultrasonics 84 (2018) 446–458, https://doi.org/10.1016/j.ultras.2017.12.007.
[56] J.K. Paul, et al., Characterization of fibromyalgia using sleep EEG signals with nonlinear dynamical features, Comput. Biol. Med. 111 (2019) 103331, https://doi.org/10.1016/j.compbiomed.2019.103331.
[57] D. Bakheet, K. Maharatna, Linear and nonlinear analysis of intrinsic mode function after facial stimuli presentation in children with autism spectrum disorder, Comput. Biol. Med. 133 (2021) 104376, https://doi.org/10.1016/j.compbiomed.2021.104376.
[58] S.A. Akar, et al., Nonlinear analysis of EEGs of patients with major depression during different emotional states, Comput. Biol. Med. 67 (2015) 49–60, https://doi.org/10.1016/j.compbiomed.2015.09.019.
[59] G. Vaziri, F. Almasganj, R. Behroozmand, Pathological assessment of patients' speech signals using nonlinear dynamical analysis, Comput. Biol. Med. 40 (1) (2010) 54–63, https://doi.org/10.1016/j.compbiomed.2009.10.011.
[60] L. Kirichenko, T. Radivilova, V. Bulakh, Generalized approach to Hurst exponent estimating by time series, Informatyka, Automatyka, Pomiary w Gospodarce i Ochronie Środowiska 8 (2018), https://doi.org/10.5604/01.3001.0010.8639.
[61] T. Di Matteo, T. Aste, M.M. Dacorogna, Long-term memories of developed and emerging markets: using the scaling analysis to characterize their stage of development, J. Bank. Finance 29 (4) (2005) 827–851, https://doi.org/10.1016/j.jbankfin.2004.08.004.
[62] T. Di Matteo, Multi-scaling in finance, Quant. Finance 7 (1) (2007) 21–36, https://doi.org/10.1080/14697680600969727.
[63] W. Caesarendra, et al., An application of nonlinear feature extraction-A case study for low speed slewing bearing condition monitoring and prognosis, in: 2013 IEEE/ASME International Conference on Advanced Intelligent Mechatronics, IEEE, 2013.
[64] H. Kantz, T. Schreiber, Nonlinear Time Series Analysis, vol. 7, Cambridge University Press, 2004, https://doi.org/10.1017/CBO9780511755798.
[65] A. Wolf, et al., Determining Lyapunov exponents from a time series, Phys. Nonlinear Phenom. 16 (3) (1985) 285–317, https://doi.org/10.1016/0167-2789(85)90011-9.
[66] M.T. Rosenstein, J.J. Collins, C.J. De Luca, A practical method for calculating largest Lyapunov exponents from small data sets, Phys. Nonlinear Phenom. 65 (1–2) (1993) 117–134, https://doi.org/10.1016/0167-2789(93)90009-P.
[67] S.K. Trivedi, et al., Prediction of consumers refill frequency of LPG: a study using explainable machine learning, Heliyon 10 (1) (2024) e23466.
[68] B. Zhang, S. Hu, M. Li, Comparative study of multiple machine learning algorithms for risk level prediction in goaf, Heliyon 9 (8) (2023) e19092, https://doi.org/10.1016/j.heliyon.2023.e19092.
[69] A. Tigrini, et al., On the decoding of shoulder joint intent of motion from transient EMG: feature evaluation and classification, IEEE Trans. Med. Robot. Bionics 5 (4) (2023) 1037–1044, https://doi.org/10.1109/TMRB.2023.3320260.
[70] M.S. Manuchehri, S.K. Setarehdan, A robust time delay estimation method for ultrasonic echo signals and elastography, Comput. Biol. Med. 136 (2021) 104653, https://doi.org/10.1016/j.compbiomed.2021.104653.
[71] Y. Cheng, et al., A survey of model compression and acceleration for deep neural networks, arXiv preprint arXiv:1710.09282 (2017), https://doi.org/10.48550/arXiv.1710.09282.